

## Influence of Internal Architectures of Cast AlSi10Cu5Ni1-2 on High Temperature Strength

Zahid Asghar<sup>1</sup>, Guillermo Requena<sup>1</sup>, Hans P. Degischer<sup>1</sup>, Elodie Boller<sup>2</sup>

<sup>1</sup>Institute of Materials Science and Technology, Vienna University of Technology, Karlsplatz 13/308, A-1040 Vienna, Austria

<sup>2</sup>European Synchrotron Radiation Facility, BP 220 38043 Grenoble Cédex, France

The strength of AlSi10Cu5Ni1 and AlSi10Cu5Ni2 piston alloys is studied at room temperature and at 300 °C as cast and after different spheroidization heat treatments (ST). The strength of both alloys decreases with increasing solution treatment periods and stabilizes at 4 h. The interconnectivity and contiguity of aluminides and eutectic Si present in both alloys as cast and after 4h ST are analyzed by means of synchrotron computed microtomography. The contiguity between eutectic Si and the aluminides in both alloys is conserved after ST. The AlSi10Cu5Ni2 alloy shows about 40% higher contiguity between aluminides and eutectic Si as compared to the AlSi10Cu5Ni1 alloy. The contiguity in AlSi10Cu5Ni2 retards fragmentation and spheroidization of eutectic Si resulting in larger interconnected structures of Si as compared to AlSi10Cu5Ni1 alloy after 4h ST. The decrease in strength of AlSi10Cu5Ni2 from as cast to 24h ST is significantly less than that of the AlSi10Cu5Ni1 alloy, where the interconnectivity of eutectic Si is reduced severely.

**Keywords:** Cast Al-Si alloys, elevated temperature strength, aluminides, synchrotron tomography, 3D microstructure

### 1. Introduction

Cast Al-Si alloys are widely used in automotive and aircraft components especially for cylinder heads, pistons and valve lifters. Hypo- and hypereutectic Al-Si alloys present good castability, high thermal conductivity, excellent corrosion, abrasion and wear resistance, high specific stiffness and attractive strength to weight ratio [1]. The piston alloys have to withstand gas temperatures up to 350-400 °C and thermal fatigue between room temperature and 300 °C. Therefore, high temperature strength and dimensional stabilities are important design criteria [2]. The addition of transition elements such as Ni and Cu are considered to be effective for improving high temperature strength of cast Al-Si piston alloys by forming stable aluminides [2- 5]. Aluminides, similarly to the eutectic Si, can form a highly interconnected three dimensional interpenetrating network of complex shape with a high degree of contiguity with the eutectic Si [6,7]. The interconnectivity, volume fraction and morphology of stiffer phases such as eutectic Si and aluminides embedded in Al play an important role in their load carrying capability [8- 10].

The aim of the present work is to analyze and quantify the effect of different architectures formed by the eutectic Si and the aluminides on the room and high temperature strength of cast AlSi10Cu5Ni1-2 alloys. For this, their internal architecture is studied in different thermal conditions by means of synchrotron X-ray computed tomography (sXCT).

### 2. Experimental

#### 2.1 Materials

The composition of the AlSi10Cu5Ni1 and AlSi10Cu5Ni2 piston alloys investigated is shown in Table 1. These alloys were produced by Kolbenschmidt (Germany) by industrial gravity die casting. Both alloys were investigated as cast (AC) and after spheroidization treatment (ST) at 490 °C for 20

min, 1 h, 4 h and 24 h. All the samples in AC and ST conditions were artificially overaged at 300 °C for 2 h to stabilize the microstructure prior to testing.

Table 1: Chemical composition of the alloys (in wt.%)

Alloy	Si	Cu	Ni	Fe	Mg	Mn	Al
AlSi10Cu5Ni1	10.4	4.8	0.7	0.5	0.7	0.1	Bal.
AlSi10Cu5Ni2	10.4	5.2	1.7	0.4	0.3	0.1	Bal.

Energy dispersive X-ray (EDX) microanalysis and X-ray powder diffraction were performed on the aluminides in AC and ST conditions in both alloys. The AlSi10Cu5Ni1 alloy shows  $Al_2Cu$ ,  $Al_7Cu_4Ni$ ,  $Al_8FeMg_3Si_6$  and  $Al_x(Fe, Mn)_ySi$  types of aluminides in AC and ST conditions. The AlSi10Cu5Ni2 alloy shows  $Al_2Cu$ ,  $Al_7Cu_4Ni$ ,  $Al_8FeMg_3Si_6$  and  $Al_x(Fe, Mn)_ySi$  aluminides in AC condition where the relative amounts were changed during ST.

## 2.2 Compression tests

Compression tests were carried out at a strain rate of  $10^{-3} s^{-1}$  using a high speed quenching dilatometer Bähr-T805. Compression specimens of 5 mm diameter and 10 mm length were deformed up to  $\sim 0.5$  true strain at room temperature (RT) and at 300 °C in all conditions. Two tests were performed for each condition.

## 2.3 Synchrotron X-ray computed tomography

sXCT was performed at the ID19 beamline at the ESRF [11] using an energy of 17.6 keV. The phase contrast mode was used to distinguish eutectic Si from the Al matrix. The sXCT projections were recorded by placing the camera at a distance of 39 mm behind the sample of 0.4 mm diameter. The sXCT projections were recorded by a 2D charge-coupled device camera developed at ESRF using an effective pixel size of  $(0.3 \mu m)^2$ . 1500 projections were acquired for each 3D reconstruction. The reconstructed sXCT volume has a final size of  $2048 \times 2048 \times 2048$  voxels, with a voxel size of  $(0.3 \mu m)^3$ . ImageJ was used to convert the images from 32 bit in to 8 bit and their further processing [12]. Resolve RT was used for analyzing these volumes in terms of interconnectivity [13]. sXCT was performed for different samples of both alloys in AC and 4h ST conditions.

## 3. Results

### 3.1 Compression tests

True-stress vs true-strain curves of AlSi10Cu5Ni1 and AlSi10Cu5Ni2 alloys from the compression tests at RT and 300 °C are shown in (Fig. 1a and 1b), respectively. (Fig. 1a) shows a typical strain hardening behaviour in the ST conditions of both alloys at RT. On the other hand, (Fig. 1b) shows a typical strain softening behaviour in all conditions of both types of alloys at 300 °C. The curves of the AC condition differ significantly from those of the ST conditions. The compression curves of all the ST conditions are similar and the strength level decreases by less than 20 MPa from the 20 min treated to 24 h one.

Fig. 2a) starts with similar  $\sigma_{0.2}$  for both alloys in AC condition: 175 MPa at RT and 95 MPa at 300 °C.  $\sigma_{0.2}$  at RT and at 300 °C decreases with increasing ST time for both tested alloys.  $\sigma_{0.2}$  of the AlSi10Cu5Ni2 remains on a higher level than that of the AlSi10Cu5Ni1 alloy as shown in Fig. 2a). The decrease in  $\sigma_{0.2}$  of AlSi10Cu5Ni1 at RT gradually stabilizes after 4h of ST time, while at 300 °C it stabilizes after 20 min, whereas  $\sigma_{0.2}$  of AlSi10Cu5Ni2 is stable at RT and 300 °C after 20 min ST. Fig. 2b) shows the dependence of  $\sigma_{max}$  at RT and at 300 °C on ST time for both tested alloys. The AlSi10Cu5Ni1 and AlSi10Cu5Ni2 alloys show similar trends of  $\sigma_{max}$ . At RT,  $\sigma_{max}$  increases from 310 MPa with ST, while at 300 °C  $\sigma_{max}$  decreases from 135 MPa in both alloys.

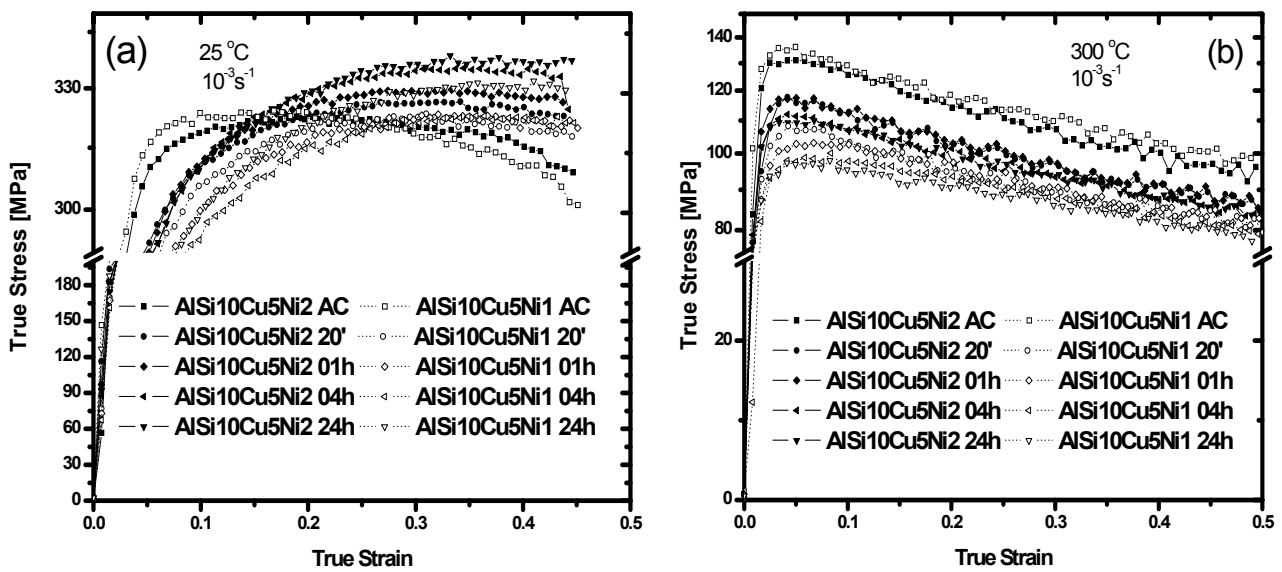


Fig. 1: True-stress vs true-strain curves obtained during compression tests for AlSi10Cu5Ni1 and AlSi10Cu5Ni2 alloys at (a) room temperature, (b) 300 °C.

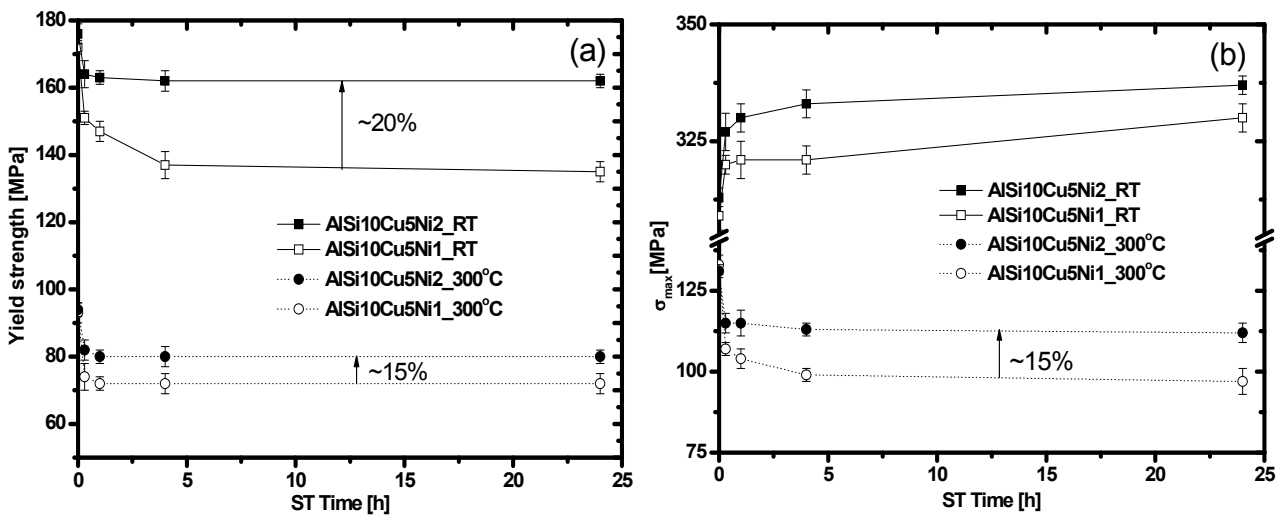


Fig. 2: (a) Compressive yield strength, (b) maximum strength at room temperature and 300 °C of AlSi10Cu5Ni1 and AlSi10Cu5Ni2 alloys in AC and ST conditions.

### 3.2 Synchrotron tomography

Fig. 3 shows cropped slices ( $0.3 \mu\text{m}$  thick) with a size of  $1076 \times 626$  pixels ( $322.8 \times 187.8 \mu\text{m}^2$ ) as an example of sXCT scans for AlSi10Cu5Ni1 and AlSi10Cu5Ni2 alloys in AC conditions. The volume fraction ( $V_f$ ) of aluminides and eutectic Si calculated from a sXCT volume of  $1076 \times 626 \times 256$  voxels =  $322.8 \times 187.8 \times 76.8 \mu\text{m}^3 \approx 0.005 \text{ mm}^3$  is shown in Table 2. The volume fraction of eutectic Si in both alloys at different conditions calculated with sXCT is close to the nominal eutectic Si content, i.e. 10.8 vol.%, (taking into account the 1.6 wt.% solubility of Si in Al and the density of Si). The error in the volume fraction of aluminides and the eutectic Si has been estimated using different threshold values for the segmentation. Table 2 also indicates the number of particles per  $\text{mm}^3$  ( $N$ ) of both phases, i.e. eutectic Si and the aluminides in both alloys in AC and 4h ST condition. Si particles less than 10000 voxels ( $270 \mu\text{m}^3$ ) were not considered neither were aluminides particles less than 2000 voxels ( $54 \mu\text{m}^3$ ). The number of particles of eutectic Si increases with ST in both alloys, but this increase is more pronounced in AlSi10Cu5Ni1 alloy with ST (see Table 2).

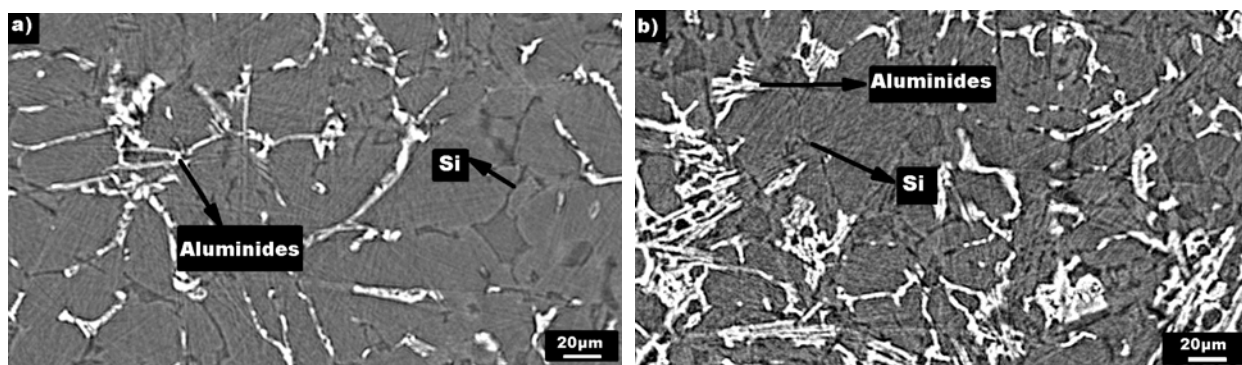


Fig. 3: Reconstructed synchrotron tomographic slice of (a) AlSi10Cu5Ni1, (b) AlSi10Cu5Ni2 AC alloys (Si: dark, aluminides: bright).

Table 2: Volume fraction and number of particles of aluminides and eutectic Si in AlSi10Cu5Ni1 and AlSi10Cu5Ni2 alloys in AC and ST condition.

Alloys	Aluminides		Eutectic Si	
	$V_f$ [%]	$N$ [ $\text{mm}^{-3}$ ]	$V_f$ [%]	$N$ [ $\text{mm}^{-3}$ ]
AlSi10Cu5Ni1-AC	$8 \pm 1$	$1.1 \times 10^4$	$9.0 \pm 1$	$1 \times 10^4$
AlSi10Cu5Ni1-4h	$8.5 \pm 1$	$1.4 \times 10^4$ (+30%)	$10.0 \pm 1$	$2.7 \times 10^4$ (+170%)
AlSi10Cu5Ni2-AC	$12.5 \pm 1$	$6 \times 10^3$	$11.0 \pm 2$	$8 \times 10^3$
AlSi10Cu5Ni2-4h	$12 \pm 1$	$8 \times 10^3$ (+30%)	$10.0 \pm 1$	$1.8 \times 10^4$ (+120%)

Interconnectivity analysis is based on the relative volume fraction of the largest particle of a certain phase with respect to the total volume fraction of that phase in the analyzed volume. Table 3 indicates the relative volume fraction of the largest Si and aluminide particles of both alloys in AC and 4h ST conditions in a volume of  $322.8 \times 187.8 \times 76.8 \mu\text{m}^3$ . There is no significant difference in the relative volume fraction of the largest aluminide particle between AC and ST conditions in both alloys. On the other hand, this difference is pronounced in the eutectic Si between AC and ST conditions, especially in the AlSi10Cu5Ni1 alloy. The largest particle of eutectic Si in AlSi10Cu5Ni1 4h ST alloy accumulates only 1/5 of the total Si content, while it accumulates 2/3 of the total Si content in AlSi10Cu5Ni2 alloy after 4h ST. This indicates that the disintegration of eutectic Si during ST is more pronounced in the AlSi10Cu5Ni1 alloy than in the alloy with 2.5 times Ni content. Fig. 4 shows 3D reconstructed volumes of all particles of eutectic Si  $>10,000$  voxels in both alloys after 4h ST condition. The different colors indicate independent Si particles with in the analyzed volume.

Contiguity is determined as the interfacial area between two different phases. Table 3 indicates the total interfacial area between eutectic Si and aluminide particles in the analyzed volume of both alloys in AC and 4h ST conditions. The contiguity area is similar in AC and ST conditions of both alloys which indicate, that contiguity between aluminides and eutectic Si is conserved during ST. AlSi10Cu5Ni1 alloy shows about 40% less contiguity area than AlSi10Cu5Ni2 alloy in the investigated volume.

Table 3 Relative volumes of the largest interconnected structures and contiguity area of Si and aluminide particles of both alloys in AC and 4h ST conditions.

Alloys	Largest Si particle	Largest aluminide particle	Largest complex Si+aluminides	Contiguity area $10^5$ ( $\mu\text{m}^2$ )
AlSi10Cu5Ni1-AC	70 %	87 %	94 %	5.8
AlSi10Cu5Ni1-4h	20 %	82 %	94 %	5.6
AlSi10Cu5Ni2-AC	80 %	97 %	97 %	9.5
AlSi10Cu5Ni2-4h	65 %	94 %	97 %	9.1

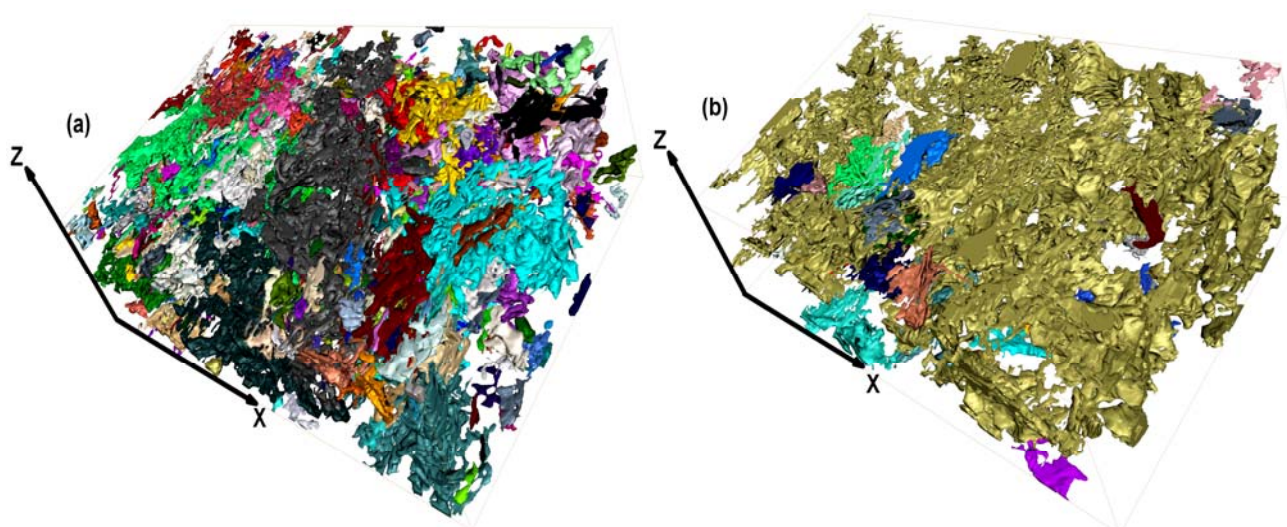


Fig. 4: Si particles  $> 10,000$  voxels in a volume of  $X = 322.8 \mu\text{m}$ ,  $Y = 187.8 \mu\text{m}$ ,  $Z = 76.8 \mu\text{m}$ . (a) in AlSi10Cu5Ni1-4h ST (b) in AlSi10Cu5Ni2-4h ST.

#### 4. Discussion

The AlSi10Cu5Ni1 and AlSi10Cu5Ni2 alloys can be considered as composites formed by the ductile  $\alpha$ -Al matrix with 18 and 22 vol.% of hybrid interpenetrating reinforcement, respectively. Both alloys show a high degree of contiguity between Si particles and aluminides in AC conditions which is maintained during ST. The larger contiguity found in the AlSi10Cu5Ni2 alloy may also depend on the volume fraction and the higher content of Ni-aluminides.

The strength of such materials is governed by: (a) the presence of hard phases with a certain aspect ratio (length to diameter ratio) providing a load transfer from Al-matrix to the reinforcement [10]; (b) the degree of interconnectivity and contiguity of the rigid phases embedded in the Al-matrix. This can result in an extra increase of load transfer, which is more important at high temperatures where the matrix is getting softer [9,14].

The high volume fraction of aluminides and larger contiguity between the aluminides and the eutectic Si in AlSi10Cu5Ni2 alloy retards the spheroidization and avoids the fragmentation of eutectic Si in comparison to the AlSi10Cu5Ni1 alloy (see Table 2). Consequently, AlSi10Cu5Ni2 alloy presents higher strength at RT and at 300 °C than AlSi10Cu5Ni1 alloy after 4 h ST (mechanism (a) and (b)).

Both the investigated alloys in AC condition show similar strength at RT and 300 °C, although AlSi10Cu5Ni2 contains about 50% higher volume fraction of aluminides and ~40% larger contiguity than AlSi10Cu5Ni1 alloy in the analyzed volume. The presence of larger contiguity and aluminides volume fraction in AlSi10Cu5Ni2 alloy may result in the early damage of the brittle network of eutectic Si and aluminides in AlSi10Cu5Ni2 alloy in AC condition causing the softening during straining. Verification of that will be the subject of future work.

#### 5. Conclusion

1. The cast AlSi10Cu5Ni1-2 alloys are formed by a ductile  $\alpha$ -Al matrix and a long range 3D interpenetrating network of aluminides and eutectic Si acting as reinforcement.
2. The contiguity between aluminides and eutectic Si is conserved with ST in both studied alloys, whereas disintegration of Si structures proceeds.
3. The higher volume fraction of aluminides and contiguity between aluminides and eutectic Si in the AlSi10Cu5Ni2 alloy reduces the fragmentation and spheroidization of Si structure during ST resulting in relatively stable structures after 20 min ST.

4. 20 min ST time seems to be enough treatment for AlSi10Cu5Ni2 piston alloys as there is only  $\pm 5\%$  difference in strength at RT and 300 °C between 20 minutes and 24h.
5.  $\sigma_{0.2}$  of the ST condition of the AlSi10Cu5Ni2 alloy is 15% and 20% higher than that of AlSi10Cu5Ni1 at 300 °C and RT, respectively.

### Acknowledgement

Z. Asghar would like to thank the Higher Education Commission (HEC), Pakistan for providing financial support for his PhD work. The authors acknowledge the company Kolbenschmidt, Germany for the provision of the alloys. The European Synchrotron Radiation Facility (ESRF) is acknowledged for the provision of synchrotron radiation access at the ID19 beamline.

### References

- 
- [1] ASM specialty handbook, Aluminium and Aluminium alloys (1994).
  - [2] Y.H. Cho, Y.R. IM, S.W. Kwon and H.C. Lee: Materials Science Forum 426-432 (2003) 339-344.
  - [3] S. Hukai, K. Takeuchi and E. Tanaka: J. Society of Materials Science, Japan; 261 (1963) 190-196.
  - [4] P. K. Rohatgi, R. C. Sharma and K.V. Prabhakar: Met. Trans. A 6A (1975) 569-575.
  - [5] J. A. García-Hinojosa, C. R. González, G. M. González and Y. Houbaert: J. Mat. Pro. Tech. 143-144 (2003) 306-310.
  - [6] Z. Asghar, G. Requena, H. P. Degischer and P. Cloetens: Acta Mat. 57 (2009) 4125-4132.
  - [7] Z. Asghar, G. Requena, E. Boller: Practical Metallography (in press)
  - [8] G. Requena, G. Garcés, M. Rodriguez, T. Pirling and P. Cloetens: Adv. Eng. Mat. 11 (2009) 1007-1014.
  - [9] G. Requena, G. Garcés, S. Danko, T. Pirling and E. Boller: Acta Mat. 57 (2009) 3199-3210.
  - [10] D. Hull and T. W. Clyne: An introduction to composite materials, Cambridge Univ. Press (2003).
  - [11] <http://www.esrf.eu/>
  - [12] <http://rsb.info.nih.gov/ij/>
  - [13] <http://www.vsg3d.com/>
  - [14] H. X. Peng, Z. Fan, D. S. Mudher and J. R. G. Evans: Mat. Sci. and Eng. A 335 (2002) 207-216.